# Multi-bit data storage using photon echoes

**Mattias Nilsson**

Master's Thesis
LRAP – 263, LTH, September 2000

# Abstract

The diffraction-limited spot size of a focused laser beam puts an upper boundary on the storage densities in conventional optical data storage. This can be overcome by storing multiple bits of data in each spatial location. In materials with an inhomogeneously broadened absorption line, such as crystals doped with rare-earth ions, frequency can be used as an additional addressing dimension. In some materials the number of spectral channels can be as high as $10^7$.

Spectral data storage can be done using coherent transient interactions between light and atoms and can be described in terms of photon echo processes. In this Master's Project the swept-carrier time-domain (SCTD) approach, a hybrid between frequency- and time-domain approaches, is used. An overview of the theory is given, followed by a description of the set-up and equipment.

A maximum of 330 bits of data have been stored in one spatial location. The necessary conditions for successful storage and retrieval of data have been examined and suggestions are given on how to extend the results further.

# Sammanfattning

Storleken på en fokuserad laserstråle begränsas av diffraktion och sätter en övre gräns för lagringstätheten i konventionell optisk datalagring. Detta kan övervinnas genom att flera bitar data sparas i varje lagringspunkt. I material som har en inhomogent breddad absorptionslinje, t.ex. kristaller som dopats med sällsynta jordartsmetaller, kan frekvens användas som en ytterligare dimension för adressering. I vissa material kan det finnas upp till $10^7$ spektrala kanaler.

Spektral datalagring kan ske genom koherent transient växelverkan mellan ljus och atomer och kan då beskrivas som en fotonekoprocess. Metoden som använts i det här arbetet utnyttjar laserljus med svept frekvens och är en hybrid mellan angreppssätt från tids- och frekvensdomänerna. En översikt över teorin ges, följd av en beskrivning av uppställning och utrustning.

Som mest lagrades 330 bitar data i en punkt. De nödvändiga villkoren för framgångsrik lagring och utläsning av data undersöktes och förslag om hur resultaten kan förbättras ges.

# Table of Contents

# 1. Introduction

Optical technology for storing, transmitting and processing information has several advantages over other technologies, such as electronic or magnetic techniques. One is that the time-scale of optical processes usually is very short and one can therefore hope to achieve considerable computing or transmission speeds. Another is that optical technology is usually less susceptible to noise or different kinds of disturbances from the surroundings.

When considering data storage, the important parameters are usually the area or volume density of the data and the rate at which data can be written and read. Optical media, such as Compact Discs, have long been inferior to magnetic storage, e.g. hard discs, and the semiconductor-based technologies used in RAMs. However, they have had the advantages of using cheap media (plastic) and straightforward techniques.

As the trend moves towards all-optical information processing, completely new ways of storing and retrieving data optically are being investigated, among them the use of frequency selective storage in inhomogeneously broadened absorber materials.

Traditionally, the number of bits that can be stored by optical means per area unit is limited by the size of the focal spot of the laser light used. The diameter of the spot is limited by diffraction to be larger than or of the order of the wavelength, $\lambda$, of the light. If one bit of data is stored per spatial location, the maximum storage density will be proportional to $1/\lambda^2$. Thus, a lot of work has been put into shifting the technology towards shorter wavelengths and by using blue ($\lambda \approx 400$ nm) lasers instead of the traditional AlGaAs lasers at around 800 nm, the optical storage density is now close to that of magnetic storage (hundreds of Mbit/cm$^2$).

Another idea is to try to store several bits at one spatial location, "multi-bit storage", and one way of doing this is to use wavelength to address bits. This can be done in materials where different groups of atoms respond to, or absorb, light at different wavelengths, which is the case for media with an inhomogeneously broadened absorption line. The idea is to use light to change the state of atoms at a certain frequency, thus changing the state of the corresponding bit between 0 and 1, and then to read out the bit by probing the state of the atoms at that frequency. The number of spectral channels that can be addressed depends on the width of the inhomogeneous profile, $\Gamma_{ih}$, and on the minimum width of a channel, which is the homogeneous linewidth, $\Gamma_h$. In some materials $\Gamma_{ih}$ is several tens of GHz, while $\Gamma_h$ is just a few kHz, which gives $10^7$ spectral channels.

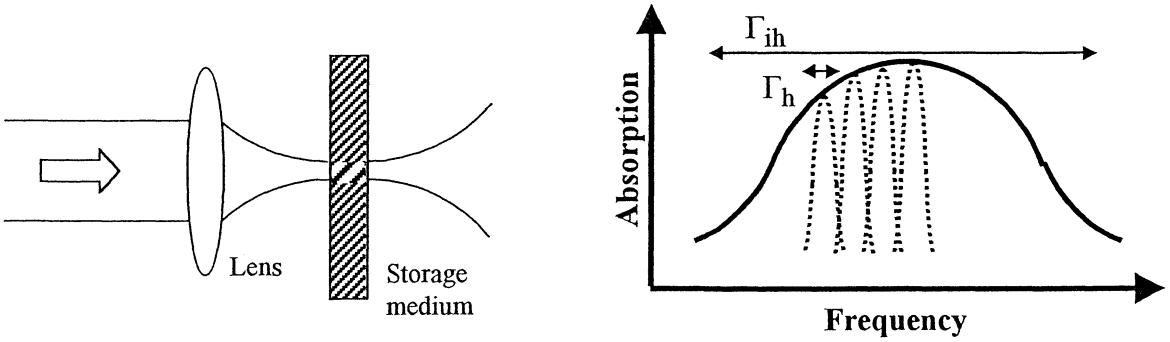


*Figure 1.1 Left: Spatial addressing of a storage cell. Right: The homogeneous absorption lines of different atoms, within the inhomogeneous absorption profile.*

The direct approach to spectral data storage is to set a tuneable laser to the appropriate wavelength and spatial position and then apply pulses to create a change in the state of the material or to read out the state. The problem with this frequency-domain approach is that if the width of a channel is of the order of kHz, your pulses need to be of the order of ms to address it, which is far to slow. (The frequency width, $\Delta\nu$, of a pulse is inversely proportional to its duration, $\Delta t$.) Broader channels means quicker access but also less data, since the number of channels equals the total inhomogeneous linewidth divided by the channel width.

The time-domain approach is a solution to this. Every sequence of pulses has a characteristic frequency content (Fourier transform) and if this can be imprinted on the absorption profile of the storage material, along with phase information, it can later be used to re-create the same sequence of pulses. This corresponds to reading or writing several spectral channels at once and makes very high data rates possible. It is necessary for the total access time to be shorter than $1/\Gamma_h$ and for the individual pulses to be longer than $1/\Gamma_{ih}$, i.e. the Fourier transform has to be contained within the inhomogeneous profile. The storage and read-out of the amplitude and phase information, corresponding to the data, can be done using transient coherent interactions and can be described in terms of photon echoes. This will be done in the following chapter.

There are several difficulties in implementing the time-domain optical memory. Firstly, one needs very high modulation and detection rates in order to utilise the full bandwidth. Secondly, the energy of the writing pulses is spread over a broad spectrum and, since the writing time is limited, one needs a powerful laser to achieve optimal intensities. Another problem is that, for reasons explained later, the output signals will have a time-dependant amplitude due to material relaxation.

This lead to the suggestion of swept-carrier time-domain optical memory (SCTDOM), which combines the best aspects of the time-domain and the frequency-domain approaches. The idea is to sweep the frequency of a tuneable laser across the absorption profile of the storage material while reading or writing, thus being able to utilise its full spectral capacity without having to access it all at once.

The objective of this diploma work was to try out the technique, using a tuneable diode laser recently constructed at the Photon Echo group at LTH. The following chapters will describe the theoretical models and the implementation. The final chapters contain a discussion of the results and some notes on the expectations on SCTDOM and variations on the idea.

For a more detailed background of the ideas presented above, see [1].

# 2. Theory

## 2.1 Photon echoes

Photon echoes are the result of a coherent and non-linear interaction between light and a medium. The simplest and most intuitively understandable form is the two-pulse photon echo (2PPE) where two light-pulses, separated by a time $\tau$, causes the material to emit a new pulse, an echo, a time $\tau$ after the second incident pulse. The three-pulse photon echo (3PPE), or stimulated echo, occurs when a third pulse illuminates the medium some time $\sigma$ after the second pulse and an echo is emitted at a time $\tau$ after this third, stimulating, pulse.

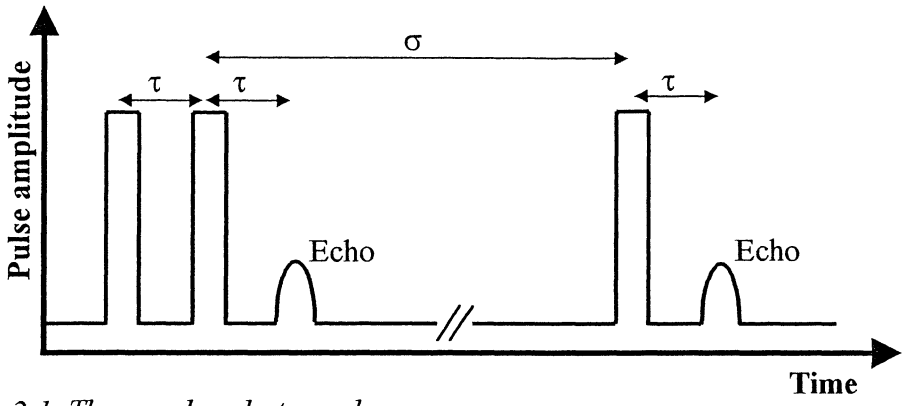


*Figure 2.1 Three-pulse photon echo.*

The phenomenon can be described in terms of four-wave mixing, where three fields interact and create a fourth field, although in this case the fields are separated in time. This is possible because of the long phase memory, or coherence time, of photon echo (PE) materials. In the case of 2PPE, the second pulse acts as both second and third field. As in four-wave mixing, the spatial dependence of photon echoes consists of a phase matching condition and conditions on the polarisation of the echoes.

The phase matching condition in the case of a 3PPE can be expressed as

$$\mathbf{k}_e = \mathbf{k}_3 + \mathbf{k}_2 - \mathbf{k}_1 \qquad (1)$$

where $\mathbf{k}_1$, $\mathbf{k}_2$ and $\mathbf{k}_3$ are the wave-vectors of the input pulses and $\mathbf{k}_e$ is the wave-vector of the echo. In the case of collinear excitation this will be fulfilled as $\mathbf{k}_1=\mathbf{k}_2=\mathbf{k}_3=\mathbf{k}_e$.

The constraints on polarisation will depend on the properties of the third order non-linear susceptibility tensor, $\chi^{(3)}$, of the material, but in many cases the polarisation of the excitation pulses and echoes will all be the same. The polarisation of the photon echoes has not been considered in this diploma work. All excitation pulses have had the same polarisation and detection has been independent of polarisation.

The time dependence of the PE process can be described in several ways, depending on which aspect one wishes to focus on and what gives the most intuitive picture of what is happening during an experiment. A full quantum mechanical description gives the correct

results even when the field intensities are high, i.e. enough for saturation, and can be illustrated using Bloch diagrams. Another description is based on the Fourier transforms of the pulses, which often makes analytic treatment easier. [2]

### 2.1.1 Quantum mechanical model

The quantum mechanical description starts by describing the atoms (or molecules) that interact with the light as two-level systems, where the state of a system, denoted $|\psi\rangle$, is written as a linear combination of the energy ground state $|g\rangle$ and an excited state $|e\rangle$

$$|\psi\rangle = c_1(t)|g\rangle + e^{-i\omega_0 t}c_2(t)|e\rangle \tag{2}$$

where the energy difference between the levels is $E = \hbar\omega_0$.
The electric field of the laser pulse is expressed classically as

$$E(\mathbf{r},t) = E_0 e^{i(\mathbf{k}\cdot\mathbf{r}-\omega t)} + c.c. \tag{3}$$

where **k** is the wave-vector of the light and ω is the angular frequency.

When a field near resonance ($\omega \approx \omega_0$) interacts with the atom, the amplitudes of the states, $c_1$ and $c_2$, changes and a polarisation, oscillating at frequency $\omega_0$, is induced. The expectation value of the dipole moment of an individual atom can be calculated as

$$\mathbf{P} = \langle\psi|\hat{\mu}|\psi\rangle = \langle\psi|-e\mathbf{r}|\psi\rangle \tag{4}$$

where $\hat{\mu}$ is the quantum dipole moment operator. The important component of a matrix-representation of $\hat{\mu}$ is

$$\mu_{eg} = \langle e|\hat{\mu}|g\rangle \tag{5}$$

which is the dipole transition moment between the ground and excited levels, and which determines how easily they can be coupled by an optical E-field.

When all individual atoms oscillate coherently, a macroscopic polarisation arises and light will be emitted with an intensity proportional to the number of atoms squared, $N^2$. Right after an exciting pulse, all atoms will oscillate in phase, but since they have slightly different resonance frequencies, due to the inhomogeneous broadening, they will dephase. A photon echo arises if a second or third excitation pulse causes the system to evolve back into a state where all atoms radiate coherently in some direction.

An excellent summary of how the interaction between light and material can be treated using density matrix formalism and Bloch vector formalism, can be found in [3].

The state of the atom, simplified to a two-level system, is described as a Bloch vector, **R**, in a diagram with three axes (u, v and w), in the following way (c.f left part of figure 2.2): The parameter w represents the population difference between the ground and the excited state. A value of −1 signifies that the atom is in the ground state and w=1 means that it is

in the excited state with probability 1. u and v represents the real and imaginary part of the optical coherence. The whole system is transformed to be rotating around the w-axis at the centre frequency of the applied field. Thus, when the atom is (partly) excited, w increases and the Bloch vector will rotate around the u-axis, from w=-1 towards w=1. When the field is turned off, the vector rotates around the w-axis with an angular frequency equal to the difference between the eigenfrequency of the atom and the frequency of the field, i.e. $\omega_0$-$\omega$. Decoherence will decrease u and v so that the vector moves towards the w-axis, while relaxation will move it towards w=-1.

In this model, the 2PPE can be described in a fairly intuitive way (c.f. right part of figure 2.2). The first pulse, at time $t_1$, should excite the atoms with a probability of 50% ($|c_1|^2=|c_2|^2=1/2$). This is equivalent to rotating the Bloch vector up into the u-v-plane (w=0). The excited atoms start to dephase, due to their different resonance frequencies, and the Bloch-vector will smear out as the vector of some atoms rotate slower around the w-axis than others. The second pulse, at time $t_2$, should rotate the Bloch vector 180° around the u-axis, flipping it back into the u-v-plane, which results in a kind of phase reversal. The atoms that were oscillating with a lower eigenfrequency and had acquired least phase now have the most phase and vice versa. The faster oscillating atoms will begin to catch up as time evolves and at time $t=t_2+(t_2- t_1)$ all atoms will be in phase again. This gives rise to a macroscopic polarisation and light is emitted. Different parts of the medium will be hit at different times by the excitation pulses and an echo will only be emitted in the direction where all macroscopic fields interfere constructively. This is what gives rise to phase-matching conditions, such as equation (1).

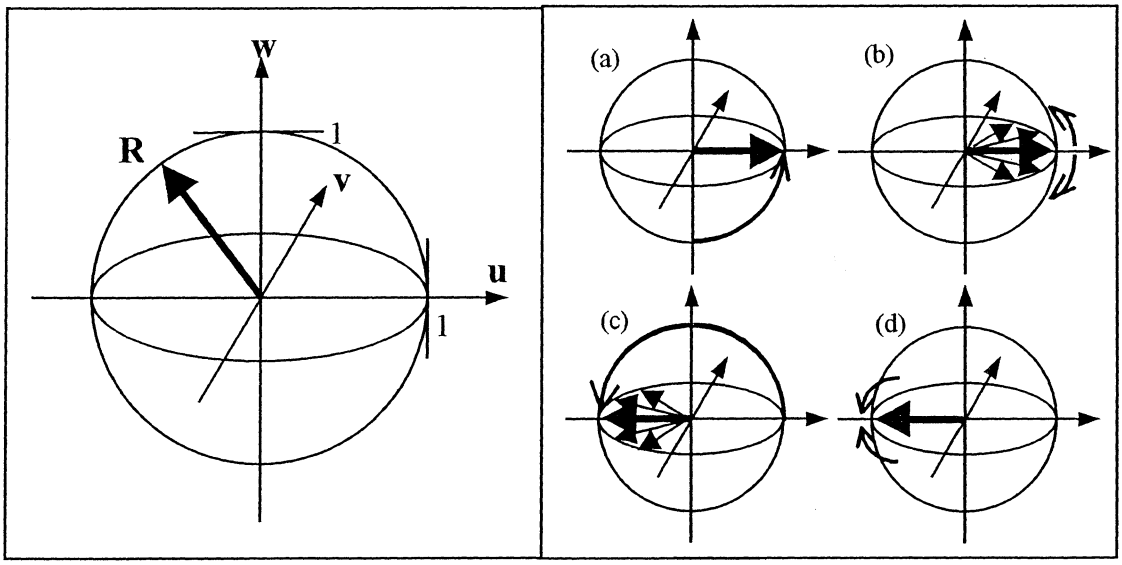


*Figure 2.2 Bloch vector diagram and 2PPE. (a) The first pulse rotates the Bloch vector into the u-v-plane. (b) Vectors corresponding to different atoms spread out, due to different $\omega_0$ . (c) The second pulse rotates the vectors around the u-axis, which causes phase differences to change sign. (d) The vectors rephase.*

A term that is often used in this context is the *pulse area*, $\theta$, of an excitation pulse. With the definition of the electric field from equation (3), it is defined as

$$\theta = \frac{2E \cdot t \cdot \mu}{\hbar} \qquad (6)$$

where E is the amplitude of the electric field, t is the duration of the pulse and $\mu$ the dipole transition moment. If all atoms are initially in the ground state ($c_1$=1 & $c_2$=0 in Eq. (2) ), the amplitudes $c_1$ and $c_2$ (Eq. (2) ) will change, after an excitation pulse, according to:

$$\begin{aligned} |c_1| &= \cos\theta/2 \\ |c_2| &= \sin\theta/2 \end{aligned} \qquad (7)$$

Thus, starting from the ground state, a $\pi/2$-pulse means that 50% of the population is put in the upper state and a $\pi$-pulse means a complete flip of population between the states. In order to maximise a 2PPE the first pulse should have the pulse area $\theta_1=\pi/2$ and the second $\theta_2=\pi$.

The 3PPE can also be described in terms of the dephasing and rephasing of partly excited populations that oscillate at different frequencies. The first pulse, with $\theta_1=\pi/2$, puts all atoms in a superposition of upper and lower state. (The Bloch vector will be rotated up into the u-v-plane). The second pulse, also with $\theta_2=\pi/2$, will excite or deexcite atoms with different resonance frequencies, depending on whether they are in phase or out of phase with the field. (The corresponding Bloch vectors are rotated around the u-axis into the u-w-plane. Depending on their phase, some atoms will be rotated towards w=1, others towards w=-1). Looking to the inhomogeneous absorption profile, this will have created a periodic "grating" in the populations of the upper and lower states, with some frequency groups excited and some in the ground state. The structure of the grating will depend on the time between the two pulses, i.e. how much time the atoms have had to dephase before the second pulse is applied. Now the coherence of the system is not essential anymore, since both phase and amplitude information about the pulses has been stored in the form of the grating. If the atoms in the excited state decay to a long-lived metastable state, the grating will still remain in the lower state. The effect of the third pulse, with $\theta_3=\pi/2$, is to put all atoms back in a superposition of states. (Put the Bloch vector back into the u-v-plane). Since only some groups of atoms, at evenly spaced frequencies, are involved they can re-phase periodically and the first time will be after a time $\tau$, equal to the time between the two first pulses. As the dipole moments of the atoms oscillate coherently, a stimulated echo is sent out.

If the description above seems difficult to grasp at first glance, the important points to remember are that the echoes are due to the phase-memory of the system and the inhomogeneous broadening of an optical transition, that lets atoms have slightly different eigenfrequencies. Information about the time between different pulses is recorded in the phases of the atoms or as a grating in the populations of the upper and lower state. If atoms can decay to a third, metastable, state the information can be stored for some time as a spectral grating in the ground state.

### 2.1.2 Fourier model

Another way of analysing the process is through the Fourier transforms of the applied pulses. It is limited to the low intensity region where $\theta<<\pi/2$ [2]. The electric field is expressed as

$$E(\omega) = F\{E(t)\} = \int_{-\infty}^{\infty} E(t)e^{-i\omega t}dt \tag{8}$$

and the polarisation induced in the material by the field is

$$P(\omega) = \varepsilon_0\left(\chi^{(1)}E(\omega) + \chi^{(2)}E(\omega)^2 + \chi^{(3)}E(\omega)^3 + \ldots\right) \tag{9}$$

where $\chi^{(1)}$ is the first order susceptibility (usually of the order of unity) and $\chi^{(2)}$ and $\chi^{(3)}$ are the second and third order susceptibilities (usually much smaller). The photon echo is a third order process, with the excitation done at near resonance and using a coherent field. The polarisation, which creates the echo, is

$$P^{(3)}(\omega) = \varepsilon_0\chi_3 E(\omega)^3 \tag{10}$$

Writing the field as the sum of the three input pulses

$$\tilde{E} = \tilde{E}_1 + \tilde{E}_2 + \tilde{E}_3,\ \tilde{E}_i = E_i + E_i^* \tag{11}$$

one gets

$$\tilde{P}^{(3)} = \varepsilon_0\chi^{(3)}(\tilde{E}_1 + \tilde{E}_2 + \tilde{E}_3)^3 = \varepsilon_0\chi^{(3)}(\tilde{E}_1^*\tilde{E}_2^2 + \tilde{E}_1^*\tilde{E}_2\tilde{E}_3 + \ldots) \tag{12}$$

The two terms written out in the sum above indicate an interaction between the first and second pulse and between all three pulses, which correspond to the 2PPE and 3PPE respectively. The polarisation is related to the population density and coherence of atoms with resonance frequency ω as described above. To calculate the echo as a function of time, one takes the inverse transform of the electric field created by the polarisation above. The result of a more careful treatment, [2], shows the 3PPE to be

$$E(t) = \frac{2\mu^2 L}{\hbar^2}\int_{-\infty}^{\infty} E_1^*(\omega)E_2(\omega)E_3(\omega)\alpha(\omega)e^{i\omega t}d\omega \tag{13}$$

where μ is the dipole transition moment of the absorbing atoms, L the length of the medium and α(ω) the absorption coefficient. If the excitation pulses only cover a small part of the inhomogeneous absorption profile, α can be assumed constant, otherwise a shifting value of α will lead to distortion of the echoes.

The echo can also be described in terms of correlations (*) and convolutions (⊗) between three fields

$$E(t) \propto E_1(t) \otimes E_2(t) * E_3(t) \tag{14}$$

The Fourier model of photon echoes can be used for analysis of temporally complex pulses and chirped pulses. However, the equations above assume that there is no decoherence between the pulses, that the linewidth of the laser is small and that the intensities are moderate.

## 2.2 Time-domain spectral data storage

As described in chapter 1, the minimum storage cell that can be addressed spatially with light has dimensions of the order of the wavelength of the light, which typically means an area of 1 $\mu m^2$. This corresponds to millions of atoms and in materials with inhomogeneously broadened absorption it is possible to address sub-groups of these atoms by tuning the frequency of the laser over the inhomogeneous profile. The minimum time required to address a group of atoms is bounded by the Fourier width of the light pulses. If we assume that the intensity is modulated as a square pulse, the energy will be distributed in the frequency domain according to $(\text{sinc}\ \pi\nu T/2)^2$, where T is the length of the pulse, and the full width at half maximum (FWHM) will approximately be $\Delta\nu_{fwhm}=0.88/T$. The width of the main lobe, i.e. between the values of $\nu$ where the energy is zero, is simply $\Delta\nu=2/T$ and this relation will be used in the following.

By using channels that are only a few kHz wide one can achieve a storage density of millions of bits per storage cell, but this also means that it will take close to a ms to read out one bit and hours to read out all.

PE phenomena rely on the collective behaviour of atoms at different resonance frequencies and it is therefore possible to use the process for fast time-domain storage and to manipulate the data transfer rate. The idea is as follows:

1. A brief, but strong, reference pulse is directed into the photon echo material. The pulse should be short enough for its Fourier width to cover a considerable part of the inhomogeneous absorption profile and intense enough to excite all atoms with a probability of ½. ($\pi/2$-pulse)
2. A series of pulses, corresponding to the data, is sent into the material. The sequence of bits (pulse/no pulse) will have a characteristic Fourier transform, which will be carried as the amplitude and phase of the light. As the light interacts with the medium, atoms at different frequencies will be excited or deexcited and the Fourier transform will be stored as a modulation of the population in the upper and lower levels of the transition.
3. The data is read out by sending another brief, strong pulse into the sample to stimulate atoms in the whole inhomogeneous profile. As the atoms oscillate in and out of phase photon echo pulses are sent out, corresponding to the original data pulses.

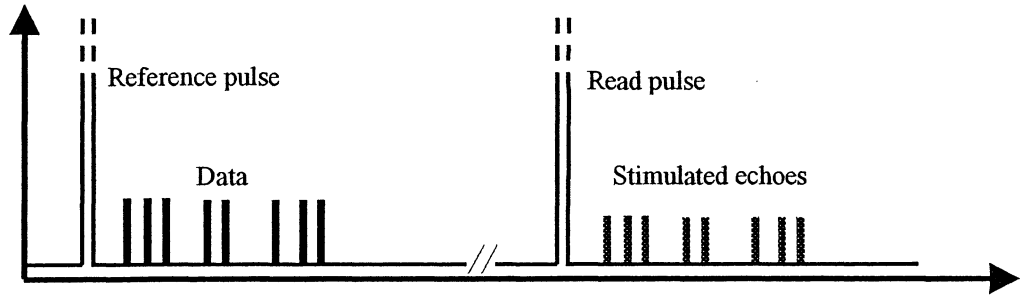


*Figure 2.3 Time domain spectral storage.*

After the initial reference pulse the data should be written within the coherence time of the material, which puts a limit on the number of bits that can be written. For $Tm^{3+}$:YAG the coherence time, $T_2$, is a few tens of $\mu s$. After this time the phases of the partially excited

atoms have no correlation and the phase information of the Fourier transform of the data cannot be recorded. This also means that the data pulses at the end of the sequence may be less faithfully recorded. The storage time, i.e. the longest time between writing and reading, is also dependent on the material and transition used. When the holeburning mechanism of $Tm^{3+}$:YAG, using a metastable state as a temporary transition state, is used it is of the order of ms.

The description above is only valid in the low intensity regime, which means that the total energy in the data pulses should correspond to less than a $\pi/2$-pulse.
The direction of the echoes is subject to the usual phase-matching conditions. (Eq. (1) )

With the time-domain approach, one can have very high data rates, but the number of bits that can be stored in one spatial location will be limited by the speed of the modulation equipment. If the write sequence does not cover the whole width of the inhomogeneous profile, one can imagine changing the centre frequency of the laser to another part of the profile and writing more data, thus using a mix of time-domain and frequency-domain techniques.

## 2.3 Swept carrier time-domain spectral data storage

Swept carrier time-domain optical memory (SCTDOM), which is the subject of this master's thesis, can be viewed as a compromise between time-domain and frequency-domain spectral storage. Like the frequency-domain approach, it can give good utilisation of the whole spectral profile and like in the time-domain approach, very high data rates can be achieved. As the name implies, the basic idea is to sweep the frequency of the laser across the absorption profile while writing or reading data. Each bit of data is only stored in a limited frequency interval, like in the frequency domain model, but the electro-magnetic field from different bits may very well interact with the same atoms, as in the time-domain model.
One advantage of the swept carrier time-domain (SCTD) approach is that pulse-areas of $\pi/2$, in the write and read pulses, can be achieved with comparatively long frequency tuned pulses, instead of the short, intense, pulses that are used in the pure time-domain approach. See for instance [4]. Another clever feature is that if the frequency off the laser beam carrying the data is shifted from the frequency of the reference beam they can both be on at the same time, since they are addressing different groups of atoms. This means that you can start writing data before the reference beam has been swept across the whole spectral region in which data is to be stored and that the duration of the data sequence can be much longer than the coherence time of the material. Experimental demonstration of this type of SCTD data storage has been achieved previously by Mossberg *et al.* [5], [6]

### 2.3.1 Principles of swept carrier time-domain optical data storage

The reference (write) beam and the data beam are focused on the spatial storage location that is to be addressed and the frequency is swept across the frequency interval available for data storage. The data beam is offset so that its carrier frequency is lagging that of the reference by a certain amount and its intensity is modulated to encode the data. The result is that the Fourier transform of the data is encoded as a population grating in the absorption profile, as described earlier, although the Fourier picture becomes somewhat more complex, since the fields are both frequency chirped and amplitude modulated.

When the data is to be read out, a read pulse, which should be a replica of the reference pulse, is sent into the sample and the data appears as a stimulated echo. If the read beam does not copy the reference perfectly, e.g. if one of them has a slightly non-linear chirp, the resulting echoes will be distorted. This can be used to manipulate the data, e.g. to change the bit-rate of the data sequence. [7], [8]

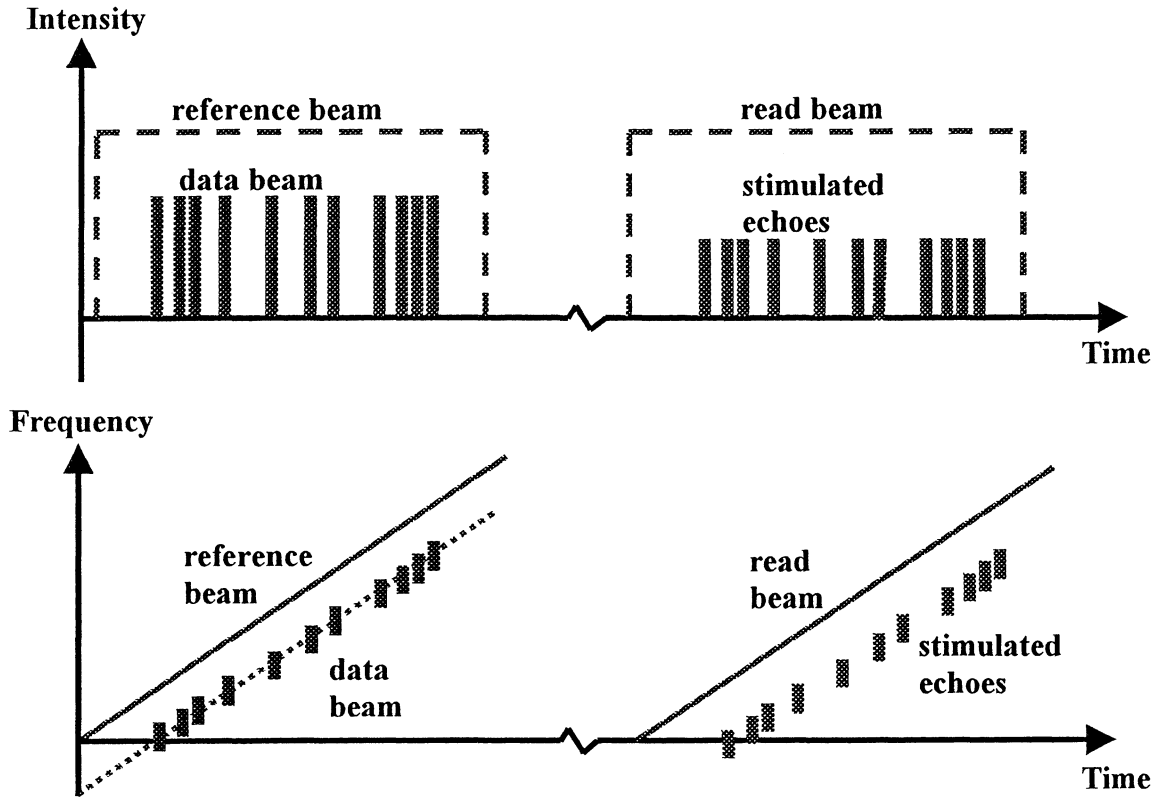


*Figure 2.4 Principles of SCTDOM. The upper picture shows the amplitudes of the excitation pulses and the resulting echoes. The lower picture shows the instantaneous frequency of the light.*

### 2.3.2 Relevant parameters

Referring to the picture above, we can introduce several important parameters:

| | |
|---|---|
| $t_b$ | Duration of one data pulse, representing a digital 1. |
| $\Delta t_b$ | Distance between the beginning of one bit and the beginning of next. The data rate is $1/\Delta t_b$. |
| $t_{seq}$ | Total duration of the data sequence. The number of stored bits is $t_{seq}/\Delta t_b$. |
| $t_{wr}$ | The time from the start of the write pulse to the start of the read pulse. |
| $\Delta\nu_{rd}$ | Frequency offset between data beam and reference beam. |
| $r_{ch}$ | Chirp rate. The rate of frequency change per time unit. If the duration of the sweep is equal to $t_{seq}$, which is usually the case, then the total frequency interval that data is stored in is $t_{seq} * r_{ch}$. |

The time $t_b$ determines the width of one bit in the Fourier domain ($\approx 2/t_b$). If $\Delta t_b * r_{ch}$ is greater than $2/t_b$ , then each bit will be stored in a separate spectral region, i.e. pure spectral storage. Much work has been dedicated to achieving high data rates and good

utilisation of the available spectral region that can be used for data storage, which means having as small $\Delta t_b$ and $r_{ch}$ as possible, while still being able to read out the data. The objective is to store as many bits as possible in one spatial location (focal spot of the laser), thus achieving high areal storage densities while having high data transfer rates.

The offset $\Delta\nu$, together with the tuning rate $r_{ch}$ , determines the time between the first excitation of a certain frequency interval, by the reference beam, and excitation by the data beam. This time is roughly equal to $\Delta\nu_{rd}/r_{ch}$, but it is important to remember that the data pulses have a certain frequency width and that parts of this frequency interval will have been excited by the reference beam at different times. $\Delta\nu_{rd}/r_{ch}$ should not be too large compared to the coherence time, $T_2$, of the PE material but, on the other hand, $\Delta\nu_{rd}$ should not be small compared to $2/t_b$ , since this would mean that the data pulses excites frequency intervals that have not yet been hit by the reference beam.

The laser puts limitations on the rate at which the frequency can be swept reliably and on the frequency region that can be covered. The rest of the equipment limits the modulation rates, detection levels and other parameters.

# 3. Set-up and equipment

## 3.1 Geometry

Data storage using photon echoes requires three EM-fields: a reference (or write) field, a temporally modulated data field, which encodes the information to be stored, and later a read field, to stimulate the emission of photon echoes and thus read out the data. All fields are created by focusing laser beams on a spot in the PE material and the echoes are collected by lenses and focused on a detector. It is most convenient, although not strictly necessary, to generate all beams with the same laser. Many different configurations are possible, as long as the beams fulfil the phase matching condition (1).

In this work, an external cavity diode laser (ECDL) was used to create frequency-chirped laser light, at around 793 nm, with a variable chirp-rate. Acousto-optic modulators (AOMs) were used to split the laser beam, modulate it temporally and to generate the frequency offset between the reference and data beams. Gold-plated mirrors were used to direct the beams and lenses, with focal lengths of between 5 and 50 cm, were used to collect and focus the light onto the sample and detector. The sample (a $Tm^{3+}$:YAG crystal) was placed inside a cryostat (Cryovac) which keeps it at a temperature around 4 Kelvin. Part of the laser light was split off directly after the laser to be analysed with a Fabry-Perot interferometer (Coherent, Spectrum Analyzer 240-2-B, 1.5 GHz FSR) and a wavelength meter [9].

Several different set-up geometries were tried, in order to get a good overlap of the interacting beams in the crystal and to minimise the background during detection of the echoes. In all of them the reference (write) and read beam followed the same path. Initially near-collinear beams were used, where the reference/read beam and the data beam entered the sample from the same direction, at a small angle. The problem with this set-up is that, since the read beam is on during the whole read-out, light from the read beam is scattered in the direction of the data beam, which causes a large background when the echoes are to be detected. Increasing the angle between the beams reduces this effect but it also reduces the volume in which the beams interact in the sample, which gives a weaker echo. The problem was avoided completely by changing to near counter-propagating geometry, where the reference/read beam and the data beam have opposite directions. (See figure 3.1). Scattered light from the read beam was negligible, but care had to be taken to avoid back reflections from the windows of the cryostat.

In the original set-up there were also two AOMs controlling each of the beams. This was thought to enhance the on/off ratio, since an AOM cannot suppress the light completely when turned off and any residual light in the data beam will interfere with the echoes. The AOMs had to be matched since each AOM gives a frequency offset of around 80 MHz and an offset of only a few MHz was needed. However, each AOM degrades the beam quality and two AOMs in series did not give a substantially higher on/off ratio, so in the later set-ups only one AOM per beam path was used.

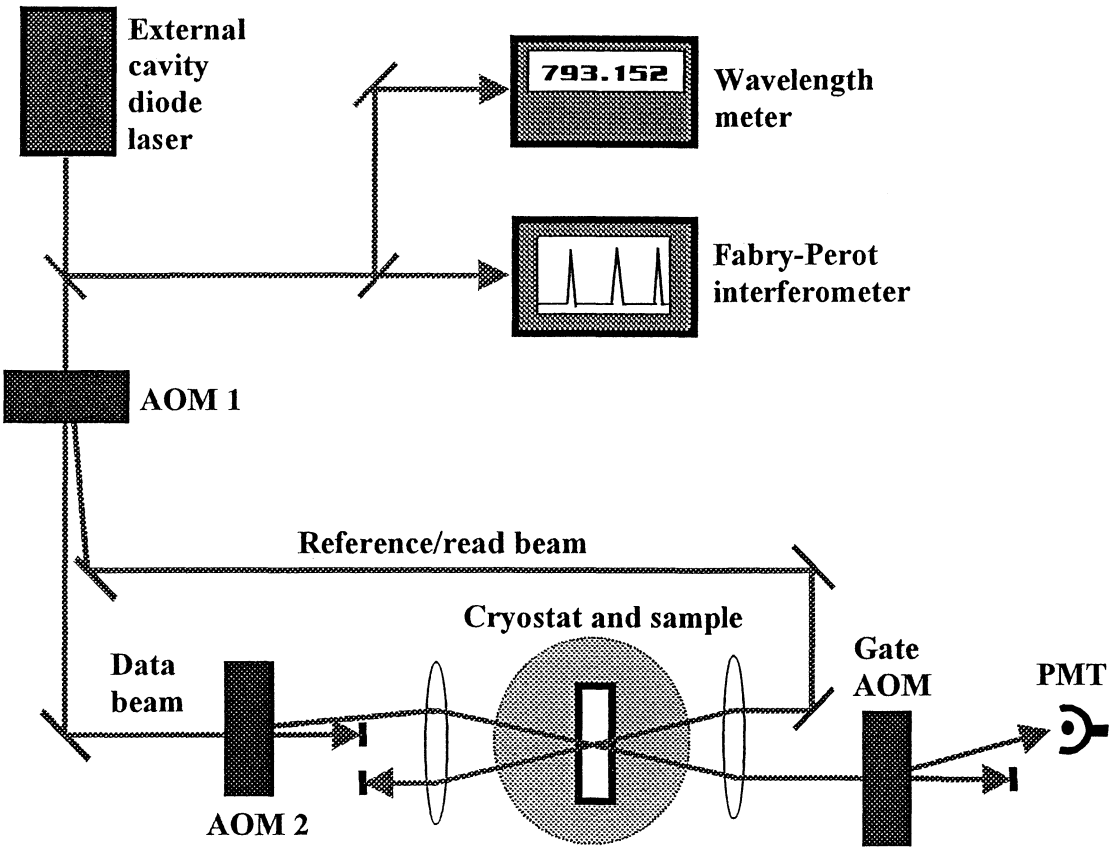


*Figure 3.1 Final set-up geometry.*

## 3.2 The photon echo material

The material that has been used is YAG (Yttrium Aluminium Garnet, $Y_3Al_5O_{12}$) doped with Thulium, Tm. The $Tm^{3+}$ ions replace $Y^{3+}$ ions in the lattice and the doping concentration is usually given as atomic percentage.

Two different $Tm^{3+}$:YAG samples were used in this work, both cylindrical with a diameter of 6 mm. One had a thickness of 1 mm and a doping concentration of 0.5 % and the other was 5 mm thick with a doping of 0.1 %.

### 3.2.1 Linewidth and coherence time

The transition of interest is the $^3H_6(1) \rightarrow {}^3H_4(1)$ transition of the trivalent Thulium ion. The centre wavelength of this absorption line was found at 793.15 nm (793.16-793.18 nm according to other research groups). The inhomogeneous linewidth is several GHz, widened by crystal strain and other effects, caused by the doping. In contrast, the homogeneous linewidth is very narrow, which corresponds to a long dephasing time, $T_2$. Under certain conditions (a temperature of 1.5 K and an applied magnetic field of $H_0$=43.8 mT) $T_2$ can be as long as 105 μs, at 3.5 K it is less than 25 μs. The lifetime of the excited state, $T_1$, is actually around 800 μs (although it decreases due to cross-relaxation when the doping concentration exceeds 0.2%) and the main cause of dephasing is coupling to the spin flipping of the $^{27}Al$ nuclei (I=5/2). [10]

Another effect that broadens the homogeneous linewidth, i.e. decreases the coherence time, appears when many ions are excited during the echo dephasing or rephasing process. When an ion is excited its dipole moment changes and this changes the local electric field experienced by nearby ions and may shift their resonance frequencies. This causes the relaxation rate and homogeneous linewidth to increase, a phenomenon known as "instantaneous spectral diffusion" [11]. When using high-power beams or tight focusing this effect must be taken into account.

### 3.2.2 Holeburning and memory time

When ions decay from the $^3H_4$ state, part of the population goes to the metastable $^3F_4$ level. This makes it possible to "burn holes" in the inhomogeneous absorption profile, by using light at selected frequencies to transfer the atoms at these frequencies to the metastable level. The hole lifetime is several ms (10 ms at 1.5 K [10]) and this will also be the longest decay time of any photon echo effects. When using the mechanism to store data one can see that the signal strength first decreases rapidly during a time period of the order of 10-100 μs, as some of the population is deexcited straight to the $^3H_6$ state, and then levels off because of the long-lived holeburning effect.

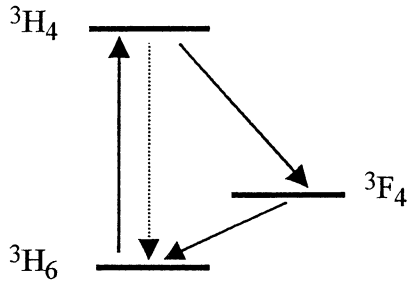

*Figure 3.2 Transitions in $Tm^{3+}$.*

### 3.2.3 Polarisation dependence

The laser light used is linearly polarised and the strength of the coupling between the $Tm^{3+}$ ions and the light will be dependent on the orientation of the crystal. The symmetry of $Tm^{3+}$:YAG is somewhat complex; YAG has the cubic space-group symmetry $O^{10}_h$ (Ia3d) and the $Tm^{3+}$ ($Y^{3+}$) sites have six different orientations. The crystal field at the sites has a $D_2$ symmetry (three orthogonal axes with 2-fold symmetry). The samples used have been cut in the [111] direction and the dipole moment of the $Tm^{3+}$ transition used have been shown to have a 6-fold symmetry when the crystal is rotated around this axis [12]. The effective dipole strength varies with less than a factor 2 when the crystal is rotated and throughout this work the crystal-holder has simply been rotated until maximum signal strength is achieved. From the data given in [12] the dipole moment of the transition can be calculated to be approximately $1.2\text{-}2.3*10^{-33}$ Cm, depending on the orientation.

### 3.2.4 Comparison to other photon echo materials

One important reason for choosing to demonstrate optical data storage in $Tm^{3+}$:YAG is that the material absorbs in a region where AlGaAs diode lasers are readily available. Another is the long coherence time, $T_2$. Photon echoes and related effects are due to coherence of the system during a sequence of applied light pulses and subsequently materials with long $T_2$ are needed in order to study them. Inorganic crystals doped with rare earth (RE) ions have very long coherence times at liquid Helium temperatures, since there are few phonons are left to cause dephasing at these low temperatures and since the transitions used are in the 4f orbital, which is shielded by 6s electrons. The transitions are between nonmagnetic electronic levels, which means that optical dephasing due to

magnetic interactions is small. YAG is a good host material since only the magnetic fluctuations of the Al nuclei contribute to the decoherence and $Tm^{3+}$ has the advantage of having nuclear spin I=1/2, which means that there are no zero-field hyperfine splittings.

Information is stored in the material through a holeburning mechanism and a long hole lifetime is therefore an advantage. There are compounds in which holes can stay more or less permanently.

There are also many photon echo materials that are cheaper and easier to manufacture than $Tm^{3+}$:YAG, e.g. different kinds of organic compounds, which are basically plastics and can be produced in a modestly equipped chemistry lab.

## 3.3 The cooling system and exposing the sample to the laser light

The PE material is cooled to 4 K inside a cryostat (Cryovac), where it is submerged in liquid Helium. It is separated from the environment by shells containing vacuum and liquid Nitrogen. The sample can be illuminated through two opposite windows, or a third window perpendicular to these. Each window has triple glass plates, which means five air(vacuum)/glass interfaces with a reflectance of around 4%, at normal incidence. This means that light passing into, or out of, the probe chamber will lose around 18% of its intensity in the passing. Part of the light will also be reflected when passing into the sample from the surrounding Helium. The refractive index of liquid Helium is $n_{l\text{-}He}$=1.408 [13] and the refractive index of YAG is $n_{YAG}$=1.82 [14], which gives a reflectance of 1.6%.

One complication is that bubbles are created in the Helium as it is heated by the laser beam and the surroundings. The gas in the bubbles has a refractive index close to 1.0, compared to 1.408 for the liquid, which means that light will be refracted and scattered by the bubbles. The effect is considered to change too slowly to effect the light during a single write-read sequence, but it means that the amplitude of the signals changes from shot to shot.

Any amplitude fluctuations have been ascribed to this and other avoidable imperfections in the set-up and, when not otherwise stated, all data has been collected from shots with good signal amplitude.

## 3.4 The modulators

The acousto-optic modulators (AOMs), used to create pulses and to shift the relative frequencies of the two beams, were ISOMET 1205C Bragg cells, driven by ISOMET D322B RF drivers. The same type of AOM was used as a gate for the detector. One of the Bragg cells was anti-reflection coated for use around 800 nm.

The driver frequency was controlled by an external voltage, $V_T$, and could be tuned between 60 MHz and 100 MHz. The AOMs were usually operated around 80 MHz, which was their optimum frequency, in terms of maximising the diffraction efficiency.

The control pulses to the AOMs were generated by a computer, or by a pulse generator (HP, 8013B) which was in turn controlled by the computer. A programmable synthesised waveform generator (SRS, DS345) was also used to create a non-uniform pulse-pattern.

### 3.4.1 Efficiency and modulation rate

In theory, the AOM can diffract all of the incident light in the 1st order, giving it a frequency offset equal to the frequency of the acoustic wave, but in practice, the maximum efficiency is 70-80%. The rise time of the beam intensity is equal to the time it takes for the acoustic wave to travel across the beam profile, so in order to get a short rise time it is necessary to focus the beam into the AOM. This decreases the efficiency, however, which means there is a trade-off between modulation speed and efficiency. The AOM is also less efficient at wavelengths around 800 nm or higher.

Another issue is the on-off ratio of the modulation. Some light will always be scattered in the direction of the 1st diffraction order and some drivers do not turn off completely when the modulation voltage is set to zero. The efficiency and modulation ratio gets worse if the beam quality is bad or when several AOMs are used in series. The on-off ratio off the drivers used was nominally better than 1000:1.

Measurements on the set-up, under favourable conditions, gave an on-off ratio of 2200:1 (2.2 mW/1.0 μw) for the data beam and 8300:1 (2.5 mW/0.3 μW) for the reference beam. The background from stray light was around 1.8 μW, using the same detector set-up.

### 3.4.2 Stability of the acousto-optic modulators

The frequency stability of the drivers was given to be ±0.25% (±0.2 MHz at 80 MHz). Since it was important that the AOMs did not introduce any variations in frequency and that the frequency offset between the reference beam and the data beam remained constant, the stability was verified experimentally. The beams from AOM1 and AOM2 (reference and data beam) were made to overlap and the beatings of the light intensity were detected with a photo diode. The signal was stored on an oscilloscope and transferred to a computer, where it was analysed using running-window Fourier transforms. (See section 3.5.2) The results showed that the AOMs were frequency-stable to within the accuracy of the measurements and computations done. Using a window of 200 μs when doing the Fourier transformation showed that the frequency varied with less than 5kHz during 1 ms. Measuring on 2 μs long pulses showed that the AOM frequency was the same from pulse to pulse, within the Fourier limit, 0.5 MHz.

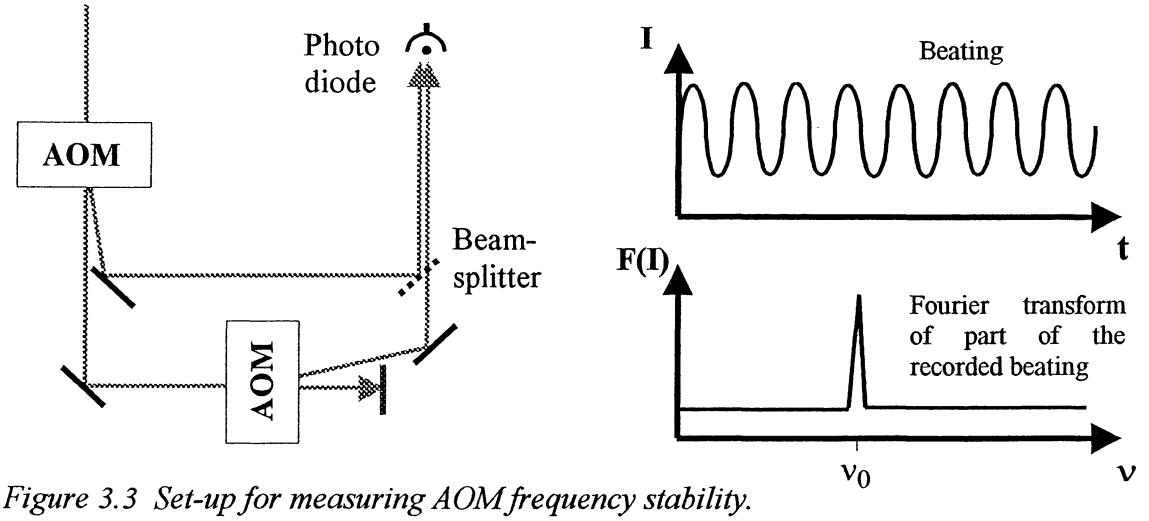


*Figure 3.3 Set-up for measuring AOM frequency stability.*

## 3.5 The external-cavity diode laser

The laser system that has been used was designed, as a diploma project, specifically for doing photon echo experiments at 793 nm, which is the transition wavelength for $Tm^{3+}$:YAG. Its most important feature is that the frequency can be tuned quickly (>54 MHz/μs) and over a wide range (2.7 GHz without mode-jumping) [15].

### 3.5.1 Laser construction and control

The laser diode is an anti-reflection coated GaAs/GaAlAs laser diode in a Littrow-type cavity, with a grating with 1800 lines/mm and feedback in the $-1^{st}$ diffraction order. Turning the grating selects the wavelength region for lasing and an electro-optic crystal ($LiTaO_3$) inside the cavity gives fast and precise control of the wavelength. When a voltage is applied across the crystal, its index of refraction changes and thus also the optical path-length ($l_{op} \approx 45$ mm), which changes the frequency of the laser. The voltage is supplied by an external high voltage amplifier (New Focus), which can give between –200 and +200 Volts. This gives a frequency-change of up to 2.7 GHz. A synthesised waveform generator (SRS, DS345) and an analogue function generator (Tektronix, FG504) were used to control the high voltage amplifier. The quality of the frequency chirp will depend on the linearity of the voltage ramp from the waveform generators and on the response of the amplifier and the electrodes on the crystal. The amplifier and the capacitance over the crystal can both cause ringings, which were partially avoided by low-pass filtering the beginning and end of the voltage ramps.

The mode and frequency of the laser could be further controlled by changing the temperature and driving current. The temperature of the diode was typically kept at 12-16°C and the output power was around 20 mW.

### 3.5.2 Laser linewidth and frequency stability

When doing photon echo experiments, it is important to have coherent light with a well-controlled frequency. The coherence of the laser is directly related to the linewidth. One of the major experimental difficulties when doing the experiments presented in this thesis was that the ECDL was not stable over longer periods of time. The wavelength needed constant adjustment and the beam quality was generally low. Originally, a linewidth of 300 kHz and a frequency drift of 3 MHz/50μs had been measured using spectral holeburning. As part of another diploma work, some new experiments were made to characterise the laser. [16]

In these experiments the light from the ECDL was mixed with light from a Ti:Sapphire-laser, pumped by an Argon-ion laser. The Ti:Sapphire-laser was tuned to the same frequency as the ECDL and the heterodyne beatings were detected with a photo-diode connected to a fast oscilloscope (Tektronix TDS 540, 1 GS/s). The signal was analysed using a windowed Fourier transform, so that the frequency at different times could be studied. This gave a very good picture of how the frequency of the ECDL changes with time.

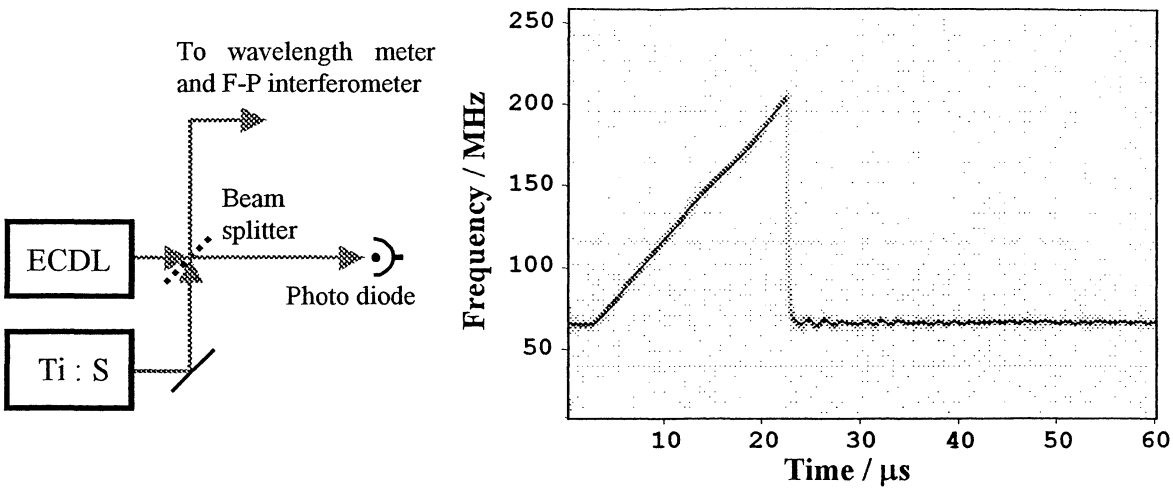


*Figure 3.4 Heterodyne detection of ECDL frequency. The right plot shows the frequency being chirped and some subsequent ringings. (Lars Levin [16])*

A number of hole-burning experiments were also made while using the same set-up. In these a "hole" is first burnt in the absorption profile, by letting a long pulse transfer all atoms with a certain resonance frequency to a metastable state, after which the frequency is scanned using an AOM, over the hole and the transmission monitored. The width of the hole will show how much the frequency has drifted during the first pulse and the position of the hole during the scan shows when the frequency matches that of the burn-pulse. The results showed a very good correlation with the heterodyne measurements that were done simultaneously.

Some 2PPE and 3PPE experiments were also done while using the heterodyne detection set-up above. The results will be described in section 4.1.2.

The conclusion from the measurements on the ECDL frequency was that its linewidth is around 400 kHz, corresponding to a coherence-time of 2.5 μs, and that the frequency could drift with a speed of up to 0.1 MHz/μs. [16]

## 3.6 Detection

Various kinds of photo-diodes (PD) were used to study the light during set-up and adjustment. The created photon echoes were just barely intense enough to be detected using a photo-diode without amplification. During the data storage experiments, the retrieved data sequences were detected with a photo multiplier tube (PMT), connected to a high voltage supply (Fluke) which could give up to 2 kV. This detector can, in principle, detect single photons, but in the present experiments the gain had to be limited to avoid damaging the PMT with too high currents. Since the original sequence of data pulses followed the same path as the read out data, a gate had to be placed before the PMT to avoid overload. The gate was an AOM that was only opened during the time interval when the echoes were expected. The possibility to use a mechanical shutter to block the data beam completely after writing was examined, but it was found that much of the background came from other sources and that the acoustic noise from the shutter disturbed the laser too much.

Since no external amplification was used, the signal to the oscilloscope was usually weak (~ 2-50 mV) but the signal to noise ratio was usually at least 20:1. The gate and the coupling into the PMT had to be carefully adjusted and apertures were inserted at various point in the set-up, in order to minimise the influence of stray light from the read beam and room illumination. The ratio between this constant background and the signal varied between 1:3 and 1:20.

An avalanche photo diode (APD) was also briefly used for detection, but since this did not give better results than the PMT, it was not used in the main experiments.

An alternative method of detection, which can be used with collinear reference and data beams, is detection of the heterodyne interference between the read beam and the output signals. As the light is mixed and detected using a PD, a noticeable beating will occur on the difference frequency, $\Delta\nu_{rd}$, between the beams. The beating can be isolated by using a low pass filter and mixing with the frequency of interest. This method eliminates the need for overlapping the foci of different beams and for gated detection, but extra electronics must be introduced, to amplify and filter the signal. [17]

Averaging over several shots could usually not be used in the data storage experiments. This was because the output bits shifted position slightly, from shot to shot, due to shifts in the frequency ramping of the laser. If these shifts were on the same order of magnitude as $\Delta t_b$, averaging could not be used. The problem can be avoided by using more sophisticated synchronisation methods.

# 4. Results

## 4.1 Photon echo experiments

As a way to test the set-up and models, some standard photon echo experiments were made, i.e. two or three pulses were sent into the sample and the pulses and echoes were detected with a photo-diode. Since the data storage process is very similar to the 3PPE process, it was important to understand how to get strong echoes.

### 4.1.1 Efficiency, pulse areas and decay times

The photon echo efficiency, i.e. the ratio of the intensity of the echo to the intensity of the excitation pulses, is usually around 0.5-1.0 %, when the set-up has been optimised.

Experiments were made with both samples (0.1% doping * 5 mm thickness and 0.5%*1 mm) and with lenses with different focal lengths focusing the beams on the sample. The beams were usually around 3 mm wide in front of the lenses, which for a Gaussian beam gives a focal spot diameter of 8.4 μm and 16.8 μm, for lenses with f=10 cm and f=20 cm, respectively. Since the beams were elliptical and somewhat irregular, it is probable that the spot sizes were actually larger than this. The Rayleigh length, i.e. the distance from the beam waist to the point where the intensity has dropped to 50%, is less than 1 mm in both cases (0.13 mm and 0.5 mm respectively), which means that the intensity will vary throughout the samples. It is important that the field intensities are high, since photon echoes are a third order effect, i.e. scales as $E^3$.

If the beam profile were simply a cylinder through the sample, the number of ions it interacted with would be the same for both samples, i.e. the linear absorption would be the same. With the beam profile described above, however, one would expect to get a stronger echo from the sample with higher doping, using pulses with the same length, since there are more $Tm^{3+}$ ions within the volume with high field intensity, but this was not seen. One interpretation is that in these experiments the interaction volume was more important than having a tight focus, i.e. that much of the signal comes from the region outside the focus. This could mean that atoms in the focus are experiencing a pulse area that is greater than optimal, but that this is compensated by a greater number of atoms outside the focus experiencing optimal excitation.

In the experiments where different beams have to interact in the sample to create a photon echo, the signal comes from the region where the beams overlap. If the beam-crossing angle is 80 mrad and the foci overlap perfectly, the overlap length will be less than 0.5 mm. However, it is hard to put the foci at exactly the same position and, in this case also, a significant part of the signal may come from the region outside the foci.

Eventually, lenses with f=10 cm were used before and after the cryostat and the 5 mm thick sample was selected.

The wavelength was varied and the maximum of the absorption profile was found between 793.148 nm and 793.155 nm, using the more lightly doped sample. It was noted that the

resonant wavelengths for the sample with 0.5% doping seemed to be slightly longer, 793.152-793.158 nm.

On a number of occasions measurements were made to find how long pulses, or how much energy, was needed to get a maximal echo, corresponding to a $\pi/2$-pulse. In fig. 4.1, echo amplitudes in a 3PPE, for different pulse lengths, are shown. The time between pulse 1 and 2 was $\tau$=3 μs and the time between pulse 2 and 3 was $\sigma$=10 μs. The optical power at the sample was 1.6 mW.

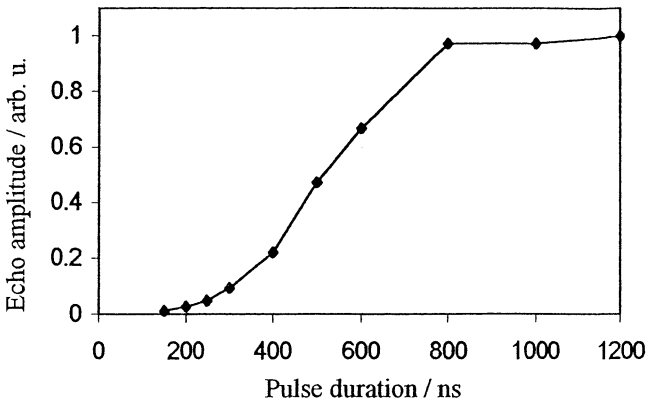


*Figure 4.1 Finding the optimal pulse area. All excitation pulses had the same duration.*

Depending on the experimental conditions, a pulse duration of around 1.0-1.5 μs, with powers of 1-3 mW, was considered to give a pulse area of $\pi/2$.
This can be compared to the following rough calculation, using a focal spot radius of 10 μm, an optical power of 2 mW and using a dipole moment of $\mu=2*10^{-33}$ Cm for the transition

$$E=\sqrt{\frac{I\cdot Z_0}{2n}}=25820\ \text{V/m},\quad \theta=\frac{2E\cdot t\cdot\mu}{\hbar}=\frac{\pi}{2}\ \Rightarrow\ t=1.6\,\mu\text{s} \qquad (15)$$

which gives an answer close to the observed value.

The shortest bit duration, $t_b$, in the data storage experiments was 80 ns, which means that the pulses were well within the linear region, and the longest $t_b$ was around 1 μs. In the latter case some ions may experience a pulse area close to $\pi/2$, if the data bits are spectrally overlapping, which means that the linear model is not applicable. The minimum amount of energy per bit that had to be used was dependent on the background, but pulses down to 80 ns*1.5 mW=120 pJ was used, although under limited circumstances.

Some experiments were made in which the distances $\sigma$ and $\tau$ between the excitation pulses was varied. By varying $\sigma$ the holeburning lifetime, i.e. the storage persistence, can be studied. By varying $\tau$, the coherence time $T_2$ can be studied as the echo decays when $\tau>T_2$.

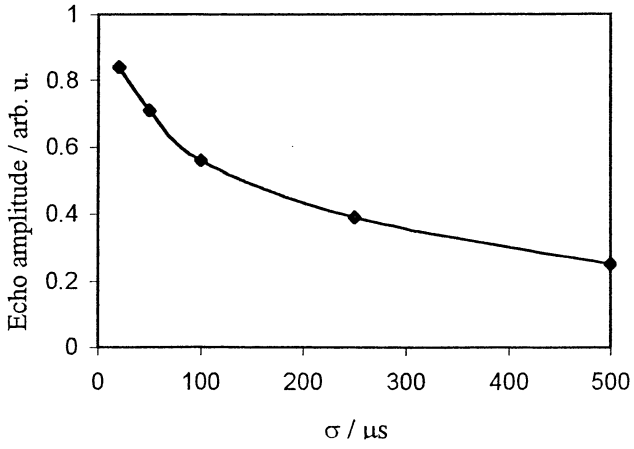


*Figure 4.2 Echo decay with storage time. $\tau$=3 μs, $\sigma$=20-500 μs.*

### 4.1.2 Correlation between laser frequency stability and photon echo efficiency

A series of PE measurements were made while the set-up for measuring the frequency of the ECDL, using heterodyne mixing, was in place. (See section 3.5.2). The influence of the frequency drift of the laser on the echo intensity was studied by recording 2PPEs and 3PPEs and laser frequency simultaneously. If the excitation pulses do not overlap in frequency, they will not interact with the same atoms and no echo will be produced. If they only overlap partially, the echo intensity will decrease, in accordance with eq. (13), which describes the echo amplitude as a convolution of the spectral contents of the excitation pulses.

The results were analysed by calculating the frequency of the ECDL at the times of the excitation pulses (figure 4.3), finding the maximum frequency difference between them and then relating the amplitude of the echoes to this. In the case of a 3PPE, the relative frequencies of all three pulses should really be taken into account, but most often only one of the pulses had a deviant frequency. The pulse length in the experiments was 700 ns, which (assuming square pulses and $\Delta\nu=2/T$) means that the pulses needed to be within 2.9 MHz of each other to overlap spectrally. The data in figure 4.4 has been re-scaled to allow for the fact that it comes from series where different values of $\tau$ and $\sigma$ have been used. The dependence on frequency difference was the same for all series and the dependence on $\tau$ and $\sigma$ is known and has been compensated for.

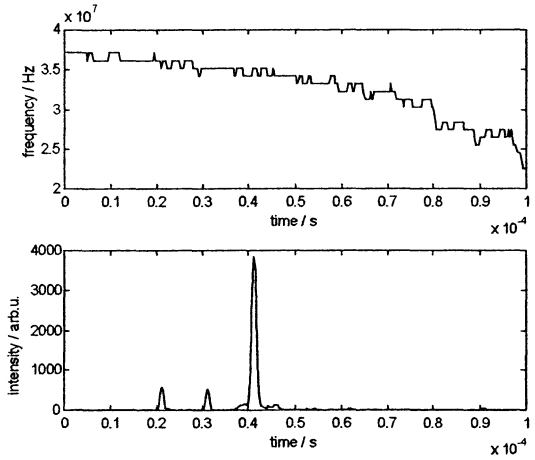


*Figure 4.3 Laser frequency and pulses in a 2PPE. The two first peaks are the excitation pulses seen through the closed gate. The frequency change between the two excitation pulses was 3.0 MHz.*

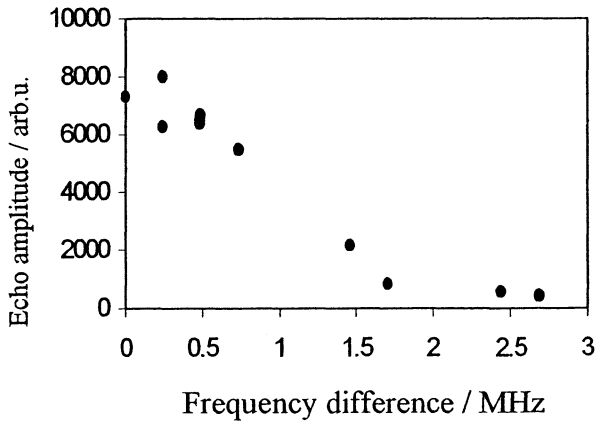


*Figure 4.4 Echo amplitude versus frequency shift between excitation pulses.*

The experiments show that the fluctuations in PE amplitude, from shot to shot, are partly due to fluctuations in laser frequency. Another source of fluctuations is bubbles in the liquid Helium, as mentioned earlier. It was shown that this effect could be reduced by pumping on the Helium, thus keeping it at a lower pressure.

Although the situation is not quite the same in a swept-carrier photon echo process, where the frequency will be swept over all intervals even though the laser has drifted, it turned out that frequency stability is an important factor for SCTD experiments also. Frequency drift leads to a varying chirp rate, which causes jitter and incorrect phase relations between atoms at different frequencies.

## 4.2 Data storage

### 4.2.1 Basic swept-carrier data storage

The first data storage experiments were made with all fields separated in time. First the reference beam was applied and chirped by 10 MHz during 10 μs, then the data beam was chirped over the same region while a number of pulses were applied. Some time later (10-100 μs) the read beam was swept over the spectral interval to stimulate the emission of echoes. The advantage of this is that it works for any geometry, since none of the beams are on when the data is to be detected, so very little interfering light will be present. The disadvantage is that data has to be written within $T_2$ from the reference sweep, which means that the data sequence cannot be longer than $T_2$.

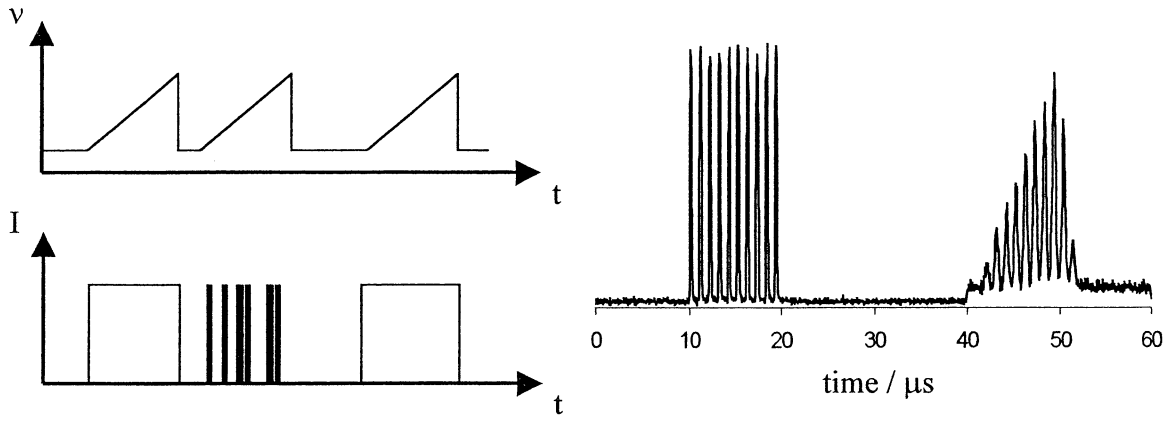


*Figure 4.5 Left: Principles of time-separated SCTD data storage. Right: Storage and recall of 10 bits by time-separated SCTD techniques. Average of 40 recordings. The first sequence is the original data pulses, detected through the closed gate, and the second sequence is the recalled data.*

Figure 4.5 shows the recording and retrieval of 10 bits of data from a point in the PE material. The reference and read pulse were from the same beam and the data beam and reference/read beam entered the sample from nearly the same direction, separated by an angle of 80 mrad. The reference and read pulse were 10 μs long and the data pulses were 700 ns long. The laser chirp rate was $r_{ch}$=1.3 MHz/μs, which gives $r_{ch} \cdot \Delta t_b$=1.3 MHz/μs·1.0 μs = 1.3 MHz. Since the Fourier width of the pulses was greater than this, they are not stored in separate spectral channels but rather as a complex Fourier transform, i.e. time-domain storage.

The varying amplitude of the bits in the output data was explained by the fact that the full Fourier spectrum of the pulses near the beginning and the end of the sweep did not fit within the sweep range. A small frequency shift, 0-5 MHz, between the reference/read and data beam, was unintentionally introduced by the AOMs and by changing this the envelope of the output pulse sequence could be translated.

When $r_{ch}$ was set to less than 0.6 MHz/μs (less than 0.6 MHz/bit) the fidelity of the recalled data decreased, as the pulses became very noisy with wildly fluctuating amplitudes. This form of "cross-talk", as the bits are packed more densely in the frequency domain, was later seen to put severe limitations on the number of bits that could be stored.

With $r_{ch}$>1.4 MHz/μs the amplitude of the read out bits decreased. This was expected, since the energy of all pulses will be spread out over a larger interval and the output amplitude is proportional to the product of the three interacting fields.

### 4.2.2 Storage of a sequence of 565 pulses and storage of 330 non-trivial data bits

Using the set-up in figure 3.1, a sequence of 565 pulses was stored, after optimising all parameters. The pulse duration was 340 ns, the time between pulses was 880 ns and the duration of the sequence was 500 μs. Note that this was several times longer than the coherence time of the material. The time between the write and read pulses was 1 ms, i.e. the read-out started 500 μs after the last data pulse. The chirp rate was 2.7 MHz / μs and the frequency offset between the beams was 2.1 MHz. The focal spot was estimated to be elliptical with diameters of 13 μm and 6.5 μm. If each pulse is taken to represent a digital 1 this would give a data storage density of 851 Mbit/cm$^2$.

The pulse sequence was not extended further for fear of overloading the PMT. Instead, the efforts were directed towards increasing the spectral storage density. In the experiment above, a frequency interval of 2.4 MHz was used for each pulse (a spectral storage density of 0.42 bits/MHz). This was much more than the homogeneous linewidth of the material and the measured linewidth of the laser, and it did not give very good projections for the maximum number of bits, considering that the laser could not be swept over more than 2.7 GHz.

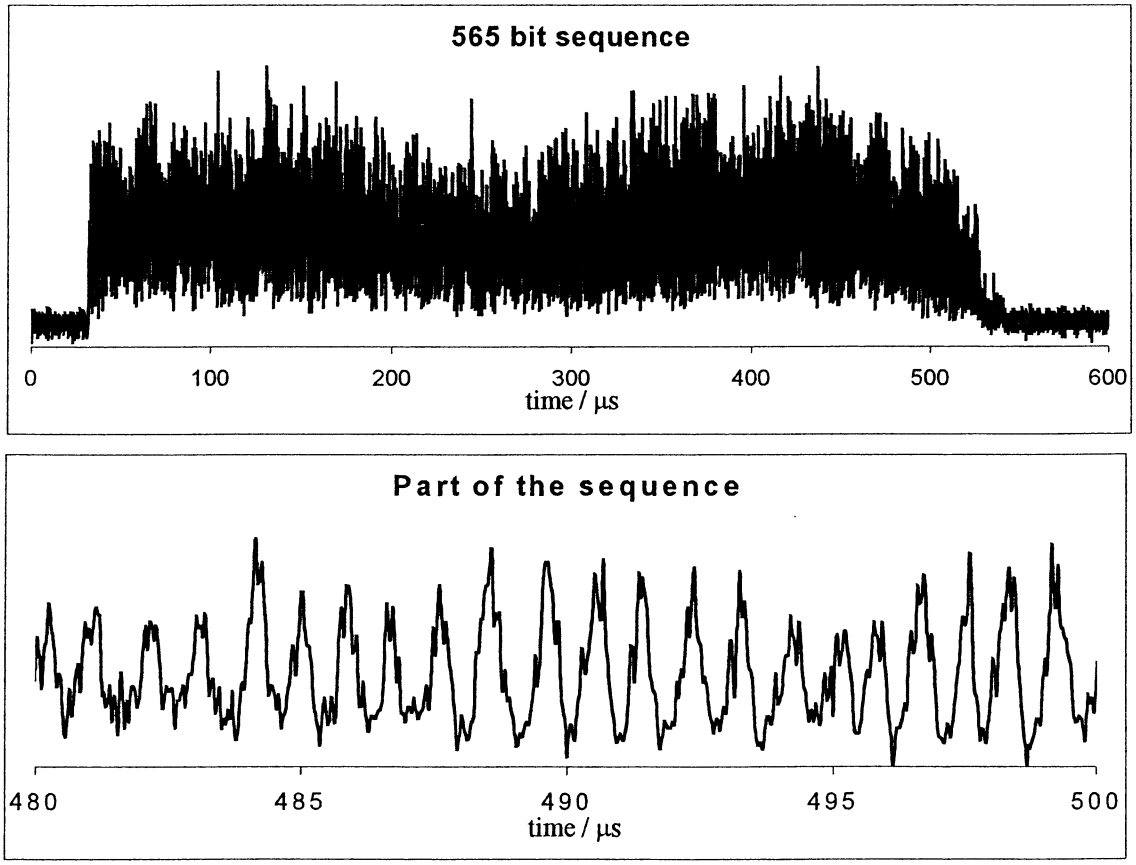


*Figure 4.6 Recall of a sequence of 565 pulses. The lower plot is an expansion of a section of the upper. $t_b$=340 ns, $\Delta t_b$=880 ns, $t_{seq}$=500 μs, $t_{wr}$=1 ms, $r_{ch}$=2.7 MHz/μs, $\Delta\nu$=2.1 MHz.*

It can be argued that storing a sequence of pulses is not true data storage, since the pattern is more regular than a random sequence of bits, and that interference between the pulses may be constructive. Therefore, the waveform- and pulse-generating electronics were later rearranged so that a more interesting bit-pattern could be stored. The 22-bit pattern was 0010001100011100011110, with the 1:s represented by light pulses. It is possible to envision an encoding where the intensity does not have to return to zero, which would mean that a series of pulses represent the bit-pattern 1010..., i.e. twice the amount of data.

The maximum amount of data that was stored in one point after changing the set-up was 330 bits (15 repetitions of the sequence). The pulse duration was 370 ns, $\Delta t_b$= 600 ns and the duration of the sequence was 200 μs. The time between the write and read pulses was 220 μs, i.e. the read-out started 20 μs after the last data pulse. The chirp rate was 2.0 MHz/μs and the frequency offset between the beams was 2.9 MHz. The data storage density was approximately 500 Mbit/cm$^2$. The spectral storage density was 0.83 bits/ MHz.

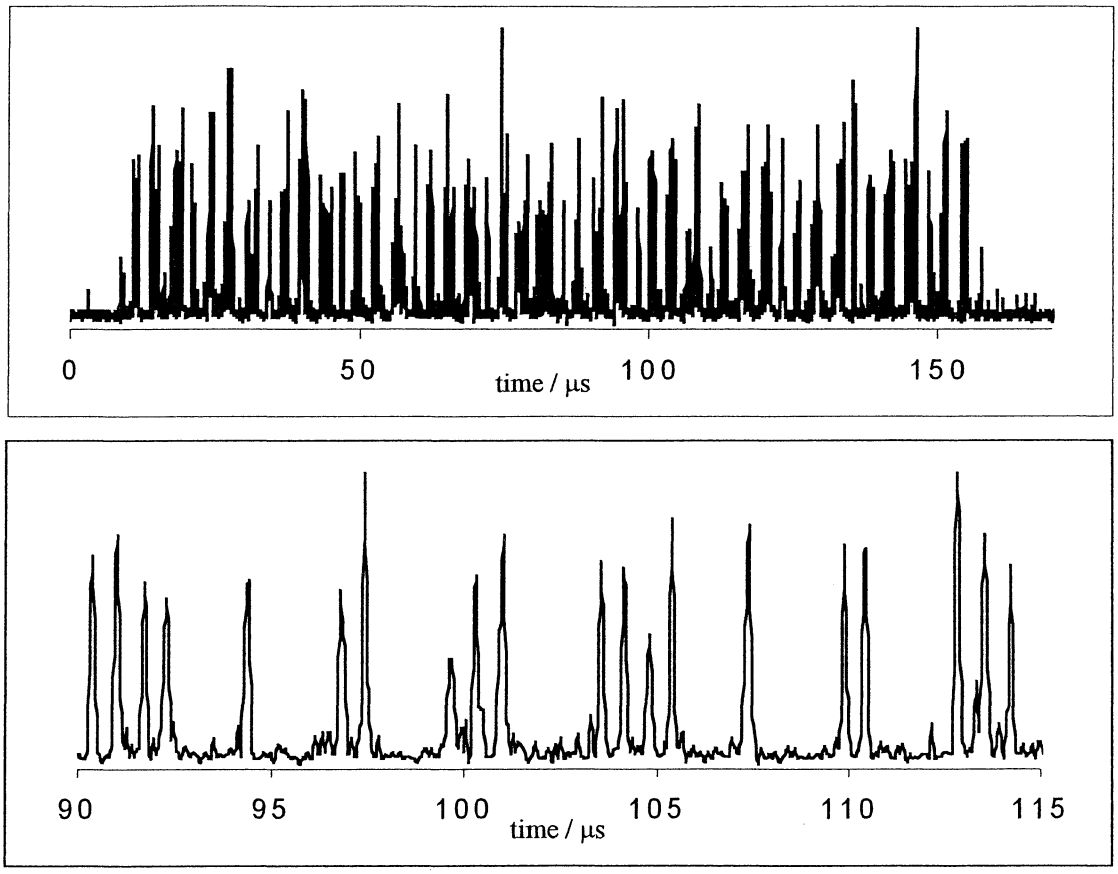


*Figure 4.7 Recall of 330 bits of data. The lower plot is an expansion of a section of the upper. $t_b$=370 ns, $\Delta t_b$=600 ns, $t_{seq}$=200 μs, $t_{wr}$=220 μs, $r_{ch}$=2.0 MHz/μs, $\Delta\nu$=2.9 MHz.*

The most probable reason why "only" 330 bits could be stored, as compared to 565 bits, is some degrading in the experimental conditions. In general, it became harder to get good results with the new set-up. The laser was performing less well, in terms of stability and beam quality, and the Tektronix function generator did not create as ideal ramps as the SRS DS345 did.

### 4.2.3 Jitter and interference between bits

Since the spectral interval that can be used for data storage is limited, primarily by the laser and eventually by the inhomogeneous linewidth, it was interesting to see how densely the bits could be packed in the frequency domain. This was done by varying the chirp rate, while keeping all other parameters constant.

Initially the product $r_{ch}*\Delta t_b$ was large enough for bits to be stored in separate frequency intervals. One could then see the effect of nonlinearities in the chirp rate as jitter in the position of the read out bits. If the chirp rate of the read pulse is slightly higher than that of the reference pulse, in a certain interval, the distance between the retrieved bits will be slightly lower than in the original data, and vice versa. In the top left picture in figure 4.8 $r_{ch}$ was 1.7 MHz/μs and $\Delta t_b$ was 2 μs, but the time between the output pulses vary from 1.8 to 2.4 μs. As the tuning rate is increased further, the jitter decreases, since the frequency fluctuations becomes less prominent, compared to the chirp.

A more interesting region is entered as $r_{ch}*\Delta t_b<1/t_b$, which means that the data pulses overlap spectrally. The state of the ions absorbing within a spectral interval will be dependent on all the data pulses that interact with that particular interval and in principle it is possible to store as many bits in an interval as the maximum number of spectral channels, determined by the ratio between the homogeneous and inhomogeneous linewidths.

Figure 4.8 shows data series where the only parameter that has been changed is the chirp rate. One can clearly see that there is a limit to how low chirp rates can be used and this was interpreted as a lower limit on the width of a spectral channel. In this case, the limit was not due to the homogeneous linewidth of the material (~40 kHz under weak excitation [5]) but the linewidth of the laser, which is inversely proportional to its coherence time. The laser must be coherent while sweeping over the interval corresponding to one bit, since atoms at different frequencies (corresponding to different parts of the bit's Fourier transform) must have a definite phase relation, in order to interfere constructively at the right instant.

The laser used had a linewidth of 300-400 kHz, which gives a coherence time of 2.5-3 μs. If, as in the left column in figure 4.8, $t_b$=500 ns, the bits span 4 MHz, which means that the chirp rate has to be at least 1.6 MHz/μs if this interval is to be swept across within the coherence time of the laser.

The right column in fig. 4.8 shows the difficulties with using pulses of short duration. $t_b$ is 100 ns, which means that the pulses span 20 MHz and that the chirp rate would have to be 8 MHz/μs, if the coherence time is 2.5 μs and all phase relations are to be correct. The chirp rate in the top right trace is 1.7 MHz/μs, which means that it takes 4-5 times the coherence time of the laser to sweep across the frequency interval corresponding to one bit. The read out echoes will broaden and deteriorate, due to the phase fluctuations.

Another conceivable reason why there is a lower limit on $r_{ch}$, is that the amount of energy per spectral interval may increase above the optimal pulse area. A chirp rate of 1 MHz/μs will cause the ions to experience a pulse area roughly equivalent to a 1 μs non-chirped pulse, during the reference and read sweeps. According to section 4.1.1 this means a pulse area of $\pi/2$. Since it is necessary to be in the linear, low intensity, region it will be a problem if some ions experience too great pulse areas.

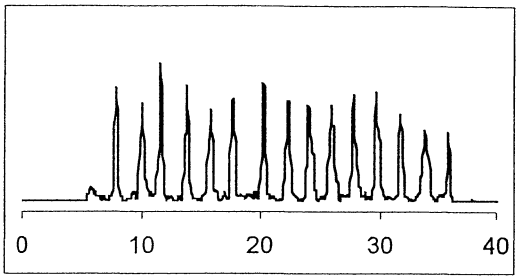


$r_{ch}$=1.70 MHz/μs $t_b$=500 ns

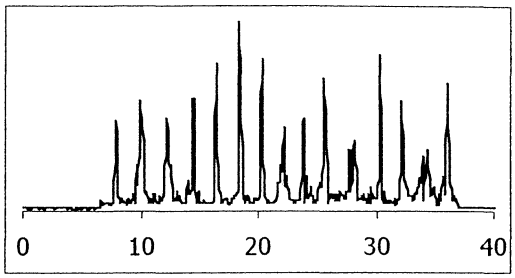


$r_{ch}$=1.70 MHz/μs $t_b$=100 ns

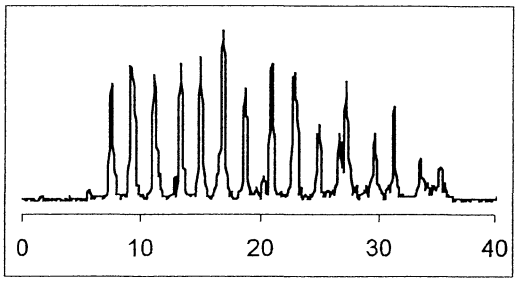


$r_{ch}$=1.35 MHz/μs $t_b$=500 ns

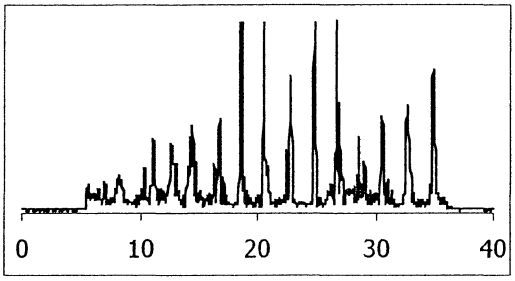


$r_{ch}$=1.35 MHz/μs $t_b$=100 ns

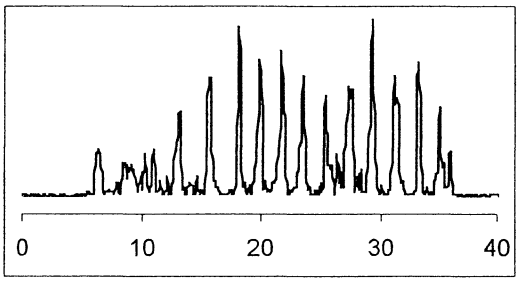


$r_{ch}$=1.15 MHz/μs $t_b$=500 ns

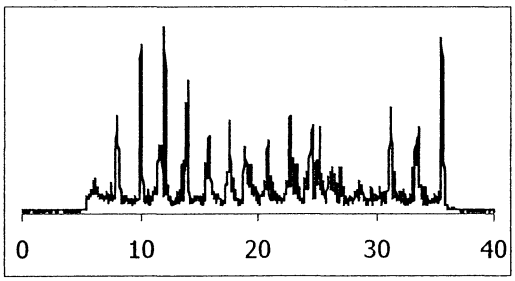


$r_{ch}$=1.15 MHz/μs $t_b$=100 ns

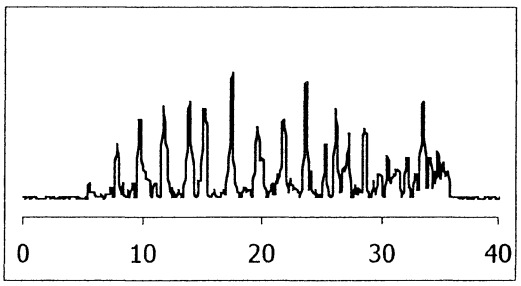


$r_{ch}$=1.10 MHz/μs $t_b$=500 ns

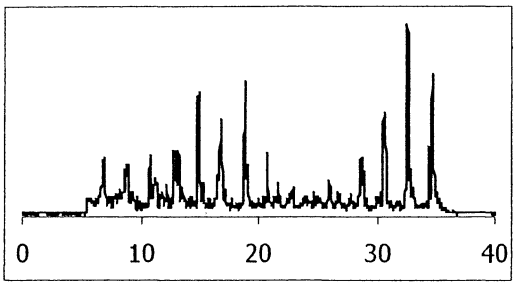


$r_{ch}$=1.10 MHz/μs $t_b$=100 ns

*Figure 4.8 Variation of jitter and output signal quality with chirp rate. The pulse duration was 500 ns in the traces in the left column and 100 ns in the right. The time between pulses was 2 μs and the chirp rate was varied between 1.1 and 1.7 MHz/μs. Note how the time between output pulses vary (jitter) and that some pulses disappear completely if the chirp rate is too slow.*

### 4.2.4 Frequency offset between reference and data waves

The frequency offset $\Delta\nu_{rd}$ was introduced by tuning the AOMs controlling the beams (AOM1 and AOM2 in figure 3.1) to slightly different frequencies. The offset could not be continuously scanned, since a change in AOM frequency led to a change in diffraction angle, which meant that the set-up had to be re-optimised. However, $\Delta\nu_{rd}$ could be changed between experiments. The maximum value of $\Delta\nu_{rd}$ that was used was 10.0 MHz (90.2 MHz-80.2 MHz) and the minimum was $\Delta\nu_{rd}$=2.1 MHz (82.1 MHz-80.0 MHz)

If the offset was too small, it was not possible to use a short bit duration, $t_b$, since the pulses would extend over frequencies that had not yet been addressed by the reference beam, which would mean problems with causality. If one assumes a full spectral pulse width of $2/t_b$, the lower limit is $\Delta\nu_{rd}>1/t_b$. It was seen that the offset could actually be made somewhat smaller than this (alternatively; the bits could be made shorter) before any destructive effect could be noticed. Note that $\Delta\nu_{fwhm}$ is only $0.88/t_b$, assuming square pulses.

In order to use short data pulses, one would wish to have a large $\Delta\nu_{rd}$, but there is an upper limit, due to the decoherence of the material. (Laser decoherence is not important in this case). The whole spectrum of a data pulse must interact with the atoms within time $T_2$ after the reference pulse has interacted with them, which gives the constraint

$$\Delta\nu_{rd} + \frac{1}{t_b} < r_{ch} \cdot T_2 \qquad (16)$$

### 4.2.5 Excitation-induced dephasing

In section 3.2.1 it was mentioned that when ions in the material are excited, the resonance frequencies of nearby ions might change, due to dipole-dipole interactions. When many ions are excited, i.e. under "massive excitation", this will cause the effective homogeneous linewidth to increase. In ref. [5] it is stated that $\Gamma_h$ in $Tm^{3+}$:YAG increased from 40 kHz, at 3.3 K and under weak excitation, to 400 kHz when around 1 GHz of the inhomogeneous profile was used for data storage. In $Eu^{3+}$:$Y_2SiO_5$, a similar PE material, $\Gamma_h$ broadens by 0.8 kHz for each MHz interval of the inhomogeneous profile that is fully excited. [18] Thus excitation-induced dephasing may become a limiting factor when one wishes to utilise the full absorption profile for spectral data storage, since the maximum number of spectral channels is $\Gamma_{ih} / \Gamma_h$.

Some experiments were made to see whether the effects of massive excitation were significant in the data storage experiments described in this thesis. A sequence of 44 bits (2 repetitions of the bit pattern above) was stored, with $t_b$=340 ns and $r_{ch}$=2.0 MHz/μs. The amount of excitation was varied by having the reference beam on for some time before or after the data pulses, while chirping. The duration of the reference pulse was varied from 20 μs, i.e. only exciting the interval where the bits were to be stored, to 200 μs, corresponding to an interval of 400 MHz. The optical power of the data beam was 1.8 mW and the power of the reference beam was 3.1 mW.

It was found that the signal strength, i.e. the intensity of the output data, decreased by 70% when a 400 MHz frequency interval was excited by a 3.1 mW beam, during the 200 μs

between the writing and read-out of the data. From this the line-width broadening due to excitation-induced dephasing was calculated to be 130 MHz. The signal fidelity did not decrease, i.e. the shape of the output did not change.

One way of minimising the effect of massive excitation is to use beams with as low power as possible. Another way is to first write in part of the inhomogeneous profile, then wait for ions to decay, meanwhile writing in another spatial location, then return to write in another spectral region in the first location, and so on. Thus, the number of simultaneously excited ions in one spot is never too great. [18]

# 5. Discussion

The maximum number of non-trivial bits of data that was stored in one spatial location in this diploma work was 330 bits, which gave a storage density of 500 Mbit/cm$^2$. This is comparable to a single layer DVD (~380 Mbit/cm$^2$) and the best results achieved using magnetic media (~775 Mbit/cm$^2$). However, unlike these techniques, the spectral data storage results are very far from the theoretical limit. The storage density can be further increased by common methods, such as using several layers (volume storage) and smaller focal spots (using shorter wavelengths), but more importantly, the number of bits stored in one spot can be increased enormously. With proper research efforts, it should be possible to increase the number of spectral channels used by several orders of magnitude. As mentioned in the introduction, in some materials the theoretical number of channels is as high as $10^7$.

From the present work it can be seen that there are initial gains to be made by using more advanced equipment and in some cases this is just a matter of cost or development time. An ideal laser, with a long coherence time and ideal chirp, would give an increase by an order of magnitude. Faster modulators, in combination with higher optical power and fast chirp, would give additional gains. At some occasions the risk of overloading the detector limited the data sequence length and a data increase by a factor of 1.5-2 could have been achieved by changing detector technology and increasing the sequence duration.

Eventually the limits set by the homogeneous linewidth will be reached. SCTDOM as described in this thesis will be limited by the linewidth broadening when a large fraction of the ions in the material are excited. If this is circumvented by using alternative approaches one can hope to get close to the limits set by the inherent properties of the storage material. Furthermore, material research can yield materials with more spectral channels, at higher temperatures and with longer storage times.

If frequency selective optical memories shall ever become interesting for practical use, it is important to investigate what advantages they have over traditional data storage techniques, apart from the higher storage densities. One advantage is that SCTDOMs can have very short access times and very high data rates, compared to any technique that relies on fast mechanical movement. Another is that they are all-optical, which means that they can be included in future all-optical data processing units.

# 6. Acknowledgements

I would like to thank everyone in the Photon Echo group for the help and encouragement I have been given during this project and for the many interesting discussions during coffee breaks.

Especially I would like to thank my supervisor, Stefan Kröll, for giving me the opportunity to learn more about new and fascinating areas in physics and for the help and inspiration provided.

I am grateful to all the people at the division of Atomic Physics who have helped me in one way or the other and to the people whose enthusiasm and teachings made me want to continue studying the subject.

Finally, my friends and family, who have put up with me while my mind was on other things than everyone else's and for introducing me to the world outside the lab.

# 7. References


[1] T. W. Mossberg, *Swept-Carrier Time-Domain Optical Memory: Background and general information*, Unpublished, University of Oregon (1993)

[2] U. Elman, *Investigations of issues relevant to the application of photon echoes in information technology*, Ph.D. Thesis, Lund Institute of Technology (1998)

[3] C. Nilsson, *Femtosecond optical bit multiplication by photon echoes excited with spectrally modulated laser pulses*, Master's Thesis, LRAP-213, Lund institute of Tecnology (1997)

[4] S. Kröll, L. E. Jusinski, R. Kachru, *Frequency-chirped copropagating multiple-bit stimulated-echo storage and retrieval in $Pr^{3+}$:$YAlO_3$*, Opt. Lett. **16**, 517 (1991)

[5] H. Lin, T. Wang, T. W. Mossberg, *Demonstration of 8-Gbit/in.$^2$ areal storage density based on swept-carrier frequency-selective optical memory*, Opt. Lett. **20**, 1658 (1995)

[6] H. Lin, T. Wang, G. A. Wilson, T. W. Mossberg, *Experimental demonstration of swept-carrier time-domain optical memory*, Opt. Lett. **20**, 91 (1995)

[7] M. Afzelius, *Theoretical modelling of temporal compression of optical pulses and pulse sequences using photon echoes*, Master's Thesis, LRAP-251, Lund Institute of Technology (1999)

[8] X. Wang, *Photon-echo based Optical Data Compression Using an External Cavity Diode Laser*, Master's Thesis, Lund Institute of Technology (2000)

[9] H. Hertz, L-Å. Nilsson, *Konstruktion och testning av digital våglängdsmätare*, Master Thesis, Lund Institute of Technology (1980)

[10] R. M. Macfarlane, *Photon-echo measurements on the trivalent thulium ion*, Opt. Lett. **18**, 1958 (1993)

[11] S. Kröll, E. Y. Xu, M. K. Kim, M. Mitsunaga, R. Kachru, *Intensity-dependent photon-echo relaxation in rare-earth-doped crystals*, Phys.Rev.B **41**, 11568 (1990)

[12] C. Greiner, B. Boggs, T. Loftus, T. Wang, T. W. Mossberg, *Polarisation-dependent Rabi frequency beats in the coherent response of $Tm^{3+}$ in YAG*, Phys. Rev. A **60,** 2657 (1999)

[13] Handbook of Chemistry and Physics, 74$^{th}$ ed., 6:149, CRC Press (1992)

[14] M. Armstrong, X. Zhu, J. Montgomery, R. J. D. Miller, *Novel composite structure Nd:YAG gain media for high power scaling of side-pumped configurations*, Opt. Commun. **175**, 201-207 (2000)

[15] R. Nilsson, *Konstruktion av en externkavitetsdiodlaser med snabb frekvensavstämning*, Master's Thesis, LRAP-241, Lund Institute of Technology (1998)

[16] L. Levin, *Construction and design of an electro-optically tuneable mode-hop free external cavity diode laser*, Master's Thesis, LRAP-261, Lund Institute of Technology (2000)

[17] H. Lin, T. Wang, G. A. Wilson, T. W. Mossberg, *Heterodyne detection of swept-carrier frequency-selective optical memory signals*, Opt. Lett. **20**, 928 (1995)

[18] A. E. Johnson, E. S. Maniloff, T. W. Mossberg, *Spatially distributed spectral storage*, Opt. Lett. **24**, 1526 (1999)

# Appendix. List of symbols and abbreviations

The units given are typical units, as used in this thesis.

| Symbol | Unit | Quantity |
|---|---|---|
| $t_b$ | ns | Duration of one data pulse, representing a digital 1. |
| $\Delta t_b$ | ns | Time separation between bits. |
| $t_{seq}$ | μs | Total duration of the data sequence. |
| $t_{wr}$ | μs | Time from the beginning of the write pulse to the read pulse. |
| $\Delta\nu_{rd}$ | MHz | Frequency offset between data beam and reference beam. |
| $r_{ch}$ | MHz / μs | Chirp rate. |
| $T_1$ | μs | Life-time of the excited state. |
| $T_2$ | μs | Coherence time. |
| $\tau$ | μs | Time between the 1st and 2nd excitation pulse in a 2(3)PPE. |
| $\sigma$ | μs | Time between the 2nd and 3rd excitation pulse in a 3PPE. |
| $\Gamma_h$ | kHz | Homogeneous linewidth of a resonance-/absorption-line. |
| $\Gamma_{ih}$ | GHz | Inhomogeneous linewidth of a resonance-/absorption-line. |
| E | V/m | Electric field strength. |
| $\mu$ | Cm | Dipole transition moment. |
| $\nu$ | MHz | Frequency. |
| f | cm | Focal length of a lens. |
| n | - | Index of refraction. |

| Abbreviation | Meaning |
|---|---|
| 2PPE | 2 pulse photon echo |
| 3PPE | 3 pulse photon echo, stimulated photon echo |
| AOM | Acousto-optic modulator |
| APD | Avalanche photo detector |
| ECDL | External cavity diode laser |
| PD | Photo diode |
| PE | Photon echo |
| PMT | Photo multiplier tube |
| RE | Rare-earth elements |
| SCTD | Swept carrier time domain |
| SCTDOM | Swept carrier time domain optical memory |
| FSR | Free spectral range |
| FWHM | Full width at half maximum |